A Shallow Water model for the numerical simulation of overland flow on surfaces with ridges and furrows

Ulrich Razafison[*,a], Stéphane Cordier[b], Olivier Delestre[c], Frédéric Darboux[d], Carine Lucas[b], François James[b]

[a] *Université de Franche-Comté, Laboratoire de Mathématiques, CNRS UMR 6623, 16 route de Gray, 25030 Besançon Cedex, France*
[b] *Université d'Orléans, Laboratoire MAPMO, CNRS UMR 6628, Fédération Denis Poisson, B. P. 6759, 45067 Orléans Cedex 2, France*
[c] *Université de Nice - Sophia Antipolis, Laboratoire de Mathématiques J. A. Dieudonné, UMR 6621 CNRS UNSA, Parc Valrose, 06108 Nice Cedex 2, France*
[d] *INRA, UR 0272 Science du sol, Centre de recherche d'Orléans, CS 40001, F-45075 Orléans Cedex 2, France*

Abstract

We introduce a new Shallow Water model for the numerical simulation of overland flow with furrow effects without representing them explicitly. The model is obtained by adding an anisotropic friction term that takes into account these effects to the classical Shallow Water equations.
We validate the model with numerical tests, and we compare it with the classical Shallow Water model where the furrows are explicitly and precisely described.

Key words: Overland flow, Shallow Water equations, Furrows, Friction

1. Introduction

During rainfall, overland flow on cultivated lands induces problems at the watershed scale for soil conservation (decreases soil thickness by erosion and causes nutrient loss), infrastructures (flooding and destruction of roads and buildings), preservation of water quality (drinking water) and sustainability of aquatic ecosystems (chemical pollution).

These troubles can be prevented by improving watershed management in connection with overland flow. Thus, the water flux at the outlet not only must be simulated well but also must predict the spatial distribution of the water flux and velocity over the whole watershed well. However, current hydrological models predict overland flow within small watersheds inefficiently [1, 2, 3]. In agricultural watersheds, one of the main difficulties is that flow directions are controlled not only by the topography but also by ditches along the field boundaries and by ridges and furrows created by tillage operations inside the fields. The flow pattern is clearly the result of the interaction between these objects [4], but the way they interact remains mostly unspecified. Therefore, this interaction must be better understood to better predict the spatial and temporal distributions of overland flow and to improve the decisions made by watershed managers.

In this paper, we focus on the interaction between topography and furrows, a feature encountered in almost all cultivated lands. This interaction can be seen as the interaction between three types of roughness. The topography is the roughness of the Earth and is described on Digital Elevation Maps with a horizontal resolution larger than one meter and commonly of ten meters and more. Furrows are the roughness due to agricultural practices and create a strong directional heterogeneity inside a field. They are characterized by their wavelength (one to a few decimeters), their amplitude (a few centimeters to one decimeter) and their direction. Finally, the random roughness due to soil aggregates and clods is homogeneous in space and has an amplitude of a few millimeters to about one decimeter. To our knowledge, most of the research on the interaction between roughness and flow have been dedicated to topography [5, 6] or to random roughness [7, 8, 9].

Few studies have addressed furrows, and most are concerned with the storage capacity of the furrows, i.e., the amount of water stored in the puddles created by the furrows (e.g., [10]). These studies do not consider the water flowing on the soil surfaces but rather the water stored in puddles. The few studies considering both overland flow and the furrows-topography interaction are empirical studies [4, 11]. They lead to empirical laws giving an on/off prediction: the predicted flow direction is either the direction of the topographic slope or the furrow direction, while water can flow in both directions at the same time in reality. Moreover, these laws are limited by their empirical basis.

To be of practical use, a model accounting for the effects of furrows on overland flow direction must not require an explicit representation of the furrows: such a requirement would require the use of a digital topographic map with a horizontal resolution of about one centimeter for the whole watershed, and a small watershed covers approximately one square kilometer. Such digital maps are not available and, even if available, require too

[*]Corresponding author. Tel: +33 381666397; fax: +33 381666623
Email addresses: ulrich.razafison@math.cnrs.fr (Ulrich Razafison), stephane.cordier@univ-orleans.fr (Stéphane Cordier), olivierdelestre41@yahoo.fr (Olivier Delestre), frederic.darboux@orleans.inra.fr (Frédéric Darboux), carine.lucas@univ-orleans.fr (Carine Lucas), francois.james@univ-orleans.fr (François James)

many computational resources.

The purpose of this study is to propose a model that can account for the effects of the furrows on overland flow. Numerical results are presented. The model is a first step in an attempt to predict overland flow directions controlled by furrows and topography without representing the furrows explicitly. Indeed, only average amplitude, wavelength and direction are used to characterize the furrows. In this paper, the furrow direction is kept perpendicular to the slope. Our model is based on the Shallow Water equations that are widely used to describe flows in rivers and ocean and overland, among other applications.

The outline of the paper is as follows. In the next section, we first present the Shallow Water model. Then, we propose a new model in which we add a new friction term to account for the effects of the furrows on overland flow. Section 3 describes the numerical scheme used to solve the model, and in Section 4, we present and discuss the numerical results that we obtain with our model. Conclusions are outlined in Section 5.

2. Mathematical models

The starting point is the 2D classic Shallow Water system [12] in a bounded domain Ω:

$$\begin{cases} \dfrac{\partial h}{\partial t} + \dfrac{\partial (hu)}{\partial x} + \dfrac{\partial (hv)}{\partial y} = R, \\ \dfrac{\partial (hu)}{\partial t} + \dfrac{\partial (hu^2)}{\partial x} + \dfrac{\partial (huv)}{\partial y} + gh\dfrac{\partial h}{\partial x} \\ \quad + gh\dfrac{\partial Z}{\partial x} + gk^2 h^{-1/3}|\boldsymbol{u}|u = 0, \\ \dfrac{\partial (hv)}{\partial t} + \dfrac{\partial (huv)}{\partial x} + \dfrac{\partial (hv^2)}{\partial y} + gh\dfrac{\partial h}{\partial y} \\ \quad + gh\dfrac{\partial Z}{\partial y} + gk^2 h^{-1/3}|\boldsymbol{u}|v = 0. \end{cases} \tag{2.1}$$

For $t > 0$ and $\boldsymbol{x} = (x, y) \in \Omega$, the unknowns are the water height $h = h(t, \boldsymbol{x})$ and the horizontal flow velocity $\boldsymbol{u} = \boldsymbol{u}(t, \boldsymbol{x}) = (u(t, \boldsymbol{x}), v(t, \boldsymbol{x}))^T$. Furthermore, $Z(\boldsymbol{x})$ describes the bottom topography of the domain; therefore, $h + Z$ is the level of the water surface (Figure 1). In equations (2.1), g is the acceleration due to the gravity and R is the rainfall intensity. Several studies have shown a derivation of the Shallow Water system originating from the free surface Navier-Stokes equations [13, 14, 15]. For the friction term, we choose the Manning law with k as the Manning coefficient. We also denote $\boldsymbol{q}(t, \boldsymbol{x}) = (q_x(t, \boldsymbol{x}), q_y(t, \boldsymbol{x}))^T = h(t, \boldsymbol{x})\boldsymbol{u}(t, \boldsymbol{x})$ as the water flux.

Now, we consider a rectangular domain $\Omega = \ell \times L$ and a topography Z with furrows. We suppose that the topography is an inclined plane with sinus furrows and that the geometry of the furrows is known through their amplitude and their wavelength. Note that realistic (measured) furrows are shaped slightly differently due to the existence of random roughness. However, random roughness, because it is isotropic, does not affect flow direction at the scale of the furrows. We also suppose that the furrows are perpendicular to the length of Ω with respect to y. An example of such topography is illustrated in Figure 2.

Next, we complement the problem with the following assumptions.

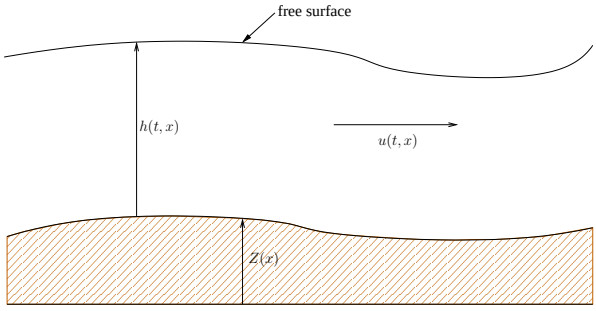

Figure 1: Notations for a 1D Shallow Water flow.

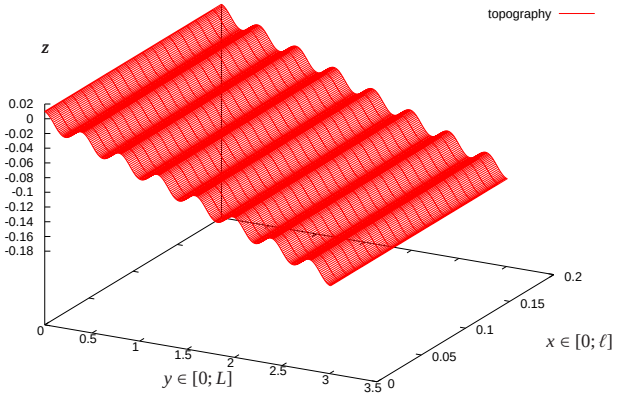

Figure 2: An example of topography with furrows.

1. The direction of the flow is parallel to the length of the domain Ω with respect to y (pseudo-1D case) and, consequently, perpendicular to the furrows.
2. We only consider fluvial flows, which means that $|\boldsymbol{u}| < \sqrt{gh}$.
3. Infiltration and soil erosion are not taken into account.

Under such assumptions, the furrows overflow at the same time during rainfall events or one after the other during inflow from upstream.

We propose a model that takes into account the effects of the furrows without explicitly representing them in the topography Z. In other words, we want to find an equivalent model to the Shallow Water system on Ω that can be used at a macroscopic scale, i.e., on a topography that is only an inclined plane. We want to force the flow to slow down when its depth is smaller than the value corresponding to the water height that can be trapped in the furrows. The idea of this article is to model this effect of the furrows through an additional friction term that forces the flow to slow down for a low water depth. To that end, we first introduce $\langle h_F \rangle$ the average height of the water trapped in the furrows. This value is given by

$$\langle h_F \rangle = V/(L_F \times \ell) \quad \text{(m)}, \tag{2.2}$$

where V is the volume of trapped water in a furrow, L_F is its wavelength (see Figure 3) and ℓ is the length of the domain Ω (with respect to x). Note that the value of $\langle h_F \rangle$ only depends on

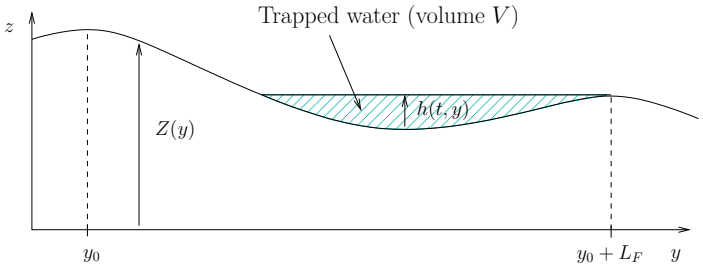

Figure 3: Water trapped in a furrow.

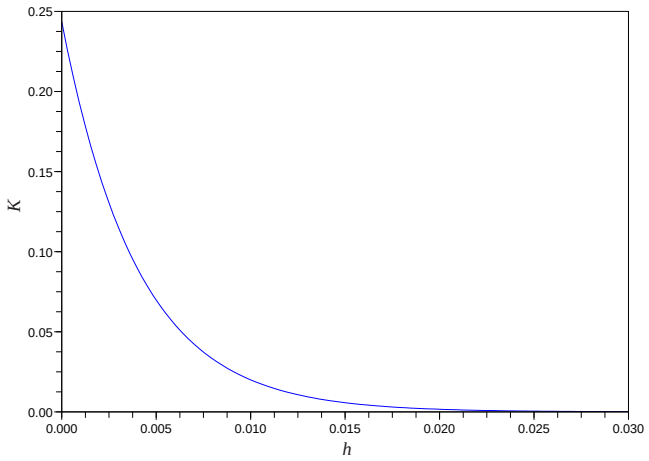

Figure 4: Shape of the friction term $K(h)$ for $\langle h_F \rangle = 0.01$ m.

three parameters: the slope of the domain, the furrows average amplitude and the furrows average wavelength.

Next, we consider the following additional friction coefficient:

$$K(h) = K_0 \exp\left(\frac{-h + \langle h_F \rangle}{C\langle h_F \rangle}\right), \tag{2.3}$$

where C is a characteristic constant increasing function of the small random variations of the height of the furrows, and K_0 is a coefficient we determine in the following.

In Figure 4, the general shape of $K(h)$ is plotted for $\langle h_F \rangle = 0.01$ m. We clearly see that $K(h)$ is large for $h \leq \langle h_F \rangle$. Thus, when the water height h is lower than the average height of the furrows $\langle h_F \rangle$, the flow slows as a result of $K(h)$,.

Remark 2.1. 1. In (2.3), if $\langle h_F \rangle$ tends to 0, then $K(h)$ also tends to 0 for any $h > 0$. In other words, the additional friction coefficient disappears when there are no furrows.

2. If C tends to 0, then we obtain the empirical models that are usually used. These models consist in giving an on/off prediction of the furrows-topography interaction (see [4, 11]); more precisely, while the critical water height is not attained, there is no flow, and after this threshold, the furrows are not taken into account.
   The new Shallow Water model we introduce here (2.4) can be seen as an improvement of these models.

Finally, we propose the following new Shallow Water model with a "furrows-friction" coefficient:

$$\begin{cases} \dfrac{\partial h}{\partial t} + \dfrac{\partial (hu)}{\partial x} + \dfrac{\partial (hv)}{\partial y} = R, \\ \dfrac{\partial (hu)}{\partial t} + \dfrac{\partial (hu^2)}{\partial x} + \dfrac{\partial (huv)}{\partial y} + gh\dfrac{\partial h}{\partial x} \\ \quad + gh\dfrac{\partial Z}{\partial x} + gk^2 h^{-1/3}|\boldsymbol{u}|u = 0, \\ \dfrac{\partial (hv)}{\partial t} + \dfrac{\partial (huv)}{\partial x} + \dfrac{\partial (hv^2)}{\partial y} + gh\dfrac{\partial h}{\partial y} \\ \quad + gh\dfrac{\partial Z}{\partial y} + gk^2 h^{-1/3}|\boldsymbol{u}|v + K(h)hv = 0. \end{cases} \tag{2.4}$$

Remark 2.2. 1. Note that, because the furrows are perpendicular to the slope, the additional friction law $K(h)hv$ only appears in the third equation of (2.4), and therefore, it only acts on the flow in the y-axis direction. This assumption is not restrictive: in general, the direction of the furrows is constant on each agricultural field, and, if necessary, we apply a rotation to obtain the equations for an arbitrary direction of the furrows.

2. The form of the new friction law is chosen arbitrarily. The general form of friction laws is $Kh^\alpha|\boldsymbol{u}|^\beta\boldsymbol{u}$ where α and β are positive real numbers. For example, we obtain the Manning law for $(\alpha,\beta) = (-1/3, 1)$ and Darcy-Weisbach law for $(\alpha,\beta) = (1, 1)$. Note that these laws are empirical and are obtained considering stationary flows, and their validity is still discussed among hydrologists (e.g., [16]).
   For the numerical experiments presented in Section 4 with system (2.4), we chose $(\alpha,\beta) = (1, 0)$ but we could have made another choice, should we change the value of K_0 or the form of $K(h)$.

Because shallow water flows can also be described by the so-called multi-layer Shallow Water system (e.g., [17, 18, 19] for a derivation and numerical studies), we can propose another approach based on multi-layer models to take into account the effects of the furrows on overland flows.

In this work, we introduce the following two-layer like model:

$$\begin{cases} \text{if } h(t,\boldsymbol{x}) \leq \langle h_F \rangle, \text{ then } \boldsymbol{u}(t,\boldsymbol{x}) = \boldsymbol{0} \text{ and } h(t,\boldsymbol{x}) = Rt, \\ \text{if } h(t,\boldsymbol{x}) > \langle h_F \rangle, \\ \quad \text{then solve (2.1) with an inclined plane topography.} \end{cases} \tag{2.5}$$

In (2.5), the lower layer corresponds to the filling up of the furrows; note that the upper layer is active only when the furrows overflow. The initial conditions for the upper layer are then $\boldsymbol{u}(0,\boldsymbol{x}) = \boldsymbol{0}$ and $h(0,\boldsymbol{x}) = \hat{h} - \langle h_F \rangle$, where $\hat{h}$ is the water height at the overflow time. Note that in one dimension, this model provides more satisfactory results than the model (2.4) (Section 4). However, its extension to more complex two-dimensional problems requires modeling the coupling between the two layers carefully, and it is more difficult than extending the model (2.4).

3. Numerical scheme

In this section, we explain the numerical scheme we used in our numerical simulations. The Shallow Water system is not as easy to solve. In hydrology, the Mac Cormack scheme is usually used for overland flow simulation (e.g., [20, 21]). However, it is not well adapted to this system because of several problems, such as the preservation of the positivity of the water height and of the steady states or the behavior at the wet/dry interface. To that end, we used well-balanced schemes [22] based on the hydrostatic reconstruction [23, 24]. This finite volume scheme has shown to be adapted to overland flow simulation at small scales [25, 26, 27].

To make this presentation simpler, we describe the numerical scheme on the classical the one-dimensional Shallow Water model with variable topography and Manning's friction law :

$$\begin{cases} \dfrac{\partial h}{\partial t} + \dfrac{\partial (hu)}{\partial x} = R \\ \dfrac{\partial (hu)}{\partial t} + \dfrac{\partial}{\partial x}\left(hu^2 + g\dfrac{h^2}{2}\right) = -gh\dfrac{\partial Z}{\partial x} - gk^2 h^{-1/3}|u|u. \end{cases} \tag{3.6}$$

The model (3.6) can be written into a conservative form

$$\frac{\partial U}{\partial t} + \frac{\partial F(U)}{\partial x} = S_0(U) + S_f(U), \tag{3.7}$$

where

$$U = \begin{pmatrix} h \\ hu \end{pmatrix} = \begin{pmatrix} h \\ q \end{pmatrix}, \quad F(U) = \begin{pmatrix} hu \\ hu^2 + g\dfrac{h^2}{2} \end{pmatrix},$$

$$S_0(U) = \begin{pmatrix} R \\ -gh\dfrac{\partial Z}{\partial x} \end{pmatrix} \quad \text{and} \quad S_f(U) = \begin{pmatrix} 0 \\ -gk^2 h^{-1/3}|u|u \end{pmatrix}.$$

System (3.7) is discretized using the finite volume method for hyperbolic conservation laws. We introduce a space-time grid in which the space and the time steps are, respectively Δx and Δt. We set $x_i = i\Delta x$, $t^n = n\Delta t$ and $C_i =]x_{i-1/2}, x_{i+1/2}[$. We denote by U_i^n the approximation of the average of $U(t^n, x)$ over the cell C_i, namely,

$$U_i^n \simeq \frac{1}{\Delta x}\int_{C_i} U(t^n, x)dx.$$

Considering only the homogeneous part of (3.7), then the finite volume scheme is of the form

$$U_i^{n+1} - U_i^n + \frac{\Delta t}{\Delta x}(F_{i+1/2}^n - F_{i-1/2}^n) = 0,$$

where $F_{i+1/2}^n = \mathcal{F}(U_i^n, U_{i+1}^n)$ is the HLL numerical flux (e.g., [24]) through the interface between C_i and C_{i+1}. Note that the HLL flux is defined by

$$\mathcal{F}(U_l, U_r) = \begin{cases} F(U_l) & \text{if } 0 < c_1, \\ \dfrac{c_2 F(U_l) - c_1 F(U_r)}{c_2 - c_1} + \dfrac{c_1 c_2}{c_2 - c_1}(U_r - U_l) & \\ & \text{if } c_1 < 0 < c_2, \\ F(U_r) & \text{if } c_2 < 0, \end{cases}$$

where $c_1 < c_2$ are given by $c_1 = \inf\limits_{U=U_l,U_r}\left(\inf\limits_{j=1,2}\lambda_j(U)\right)$, $c_2 = \sup\limits_{U=U_l,U_r}\left(\sup\limits_{j=1,2}\lambda_j(U)\right)$ and where $\lambda_1(U) = u - \sqrt{gh}$, $\lambda_2(U) = u + \sqrt{gh}$ are the eigenvalues of the Jabobian matrix $F'(U)$. A study compared different numerical fluxes for (3.6) and showed that, in the framework of overland flow, the HLL flux is the best compromise between the accuracy of the approximation and the computational cost [27]. To have a second order accuracy scheme, we use the modified ENO reconstruction [28] defined as follows

$$\begin{aligned} h_{i-1/2+} &= h_i - \frac{\Delta x}{2}D_{enom}h_i, \qquad h_{i+1/2-} = h_i + \frac{\Delta x}{2}D_{enom}h_i, \\ u_{i-1/2+} &= u_i - \frac{h_{i+1/2-}}{h_i}\frac{\Delta x}{2}D_{enom}u_i, \\ u_{i+1/2-} &= u_i + \frac{h_{i-1/2+}}{h_i}\frac{\Delta x}{2}D_{enom}u_i \end{aligned}$$

with, for a spatially discretized function s,

$$D_{enom}s_i = \text{minmod}(D_{eno}s_i, 2\theta_{enom}D_{mm}s_i)$$

where

$$\text{minmod}(x, y) = \begin{cases} \min(x, y) & \text{if } x, y \geqslant 0 \\ \max(x, y) & \text{if } x, y \leqslant 0 \\ 0 & \text{otherwise,} \end{cases}$$

$$\begin{aligned} D_{eno}s_i &= \text{minmod}\left(\frac{s_i - s_{i-1}}{\Delta x} + \theta_{eno}\frac{\Delta x}{2}D^2 s_{i-1/2}, \right. \\ &\qquad \left. \frac{s_{i+1} - s_i}{\Delta x} - \theta_{eno}\frac{\Delta x}{2}D^2 s_{i+1/2}\right), \\ D^2 s_{i+1/2} &= \text{minmod}\left(\frac{s_{i+1} - 2s_i + s_{i-1}}{\Delta x^2}, \frac{s_{i+2} - 2s_{i+1} + s_i}{\Delta x^2}\right), \\ D_{mm}s_i &= \text{minmod}\left(\frac{s_i - s_{i-1}}{\Delta x}, \frac{s_{i+1} - s_i}{\Delta x}\right) \end{aligned}$$

with $\theta_{eno}, \theta_{enom} \in [0, 1]$. Note that for $\theta_{eno} = 0$, this reconstruction is exactly the usual MUSCL reconstruction.
To take into account the topography while preserving the steady state of a lake at rest, i.e.,

$$h + Z = cst \text{ and } u = 0,$$

we use a hydrostatic reconstruction described elsewhere [23, 24]. First, we need to define the reconstructed values $Z_{i+1/2-}$ and $Z_{i-1/2+}$ that can be deduced from the reconstructed values $h_{i-1/2-}$, $h_{i-1/2+}$ and the following reconstruction of $Z + h$:

$$(Z + h)_{i-1/2+} = Z_i + h_i - \frac{\Delta x}{2}D_{enom}(Z_i + h_i)$$

and

$$(Z + h)_{i+1/2-} = Z_i + h_i + \frac{\Delta x}{2}D_{enom}(Z_i + h_i).$$

Next the hydrostatic reconstruction requires the following new values to be defined:

$$h_{i+1/2l} = \max(0, h_{i+1/2-} + Z_{i+1/2-} - \max(Z_{i+1/2-}, Z_{i+1/2+})),$$

$$h_{i-1/2\,r} = \max(0, h_{i+1/2+} + Z_{i+1/2+} - \max(Z_{i+1/2-}, Z_{i+1/2+})),$$

$$U_{i+1/2\,l} = \begin{pmatrix} h_{i+1/2\,l} \\ h_{i+1/2\,l}\, u_{i+1/2-} \end{pmatrix}, \quad U_{i-1/2\,r} = \begin{pmatrix} h_{i-1/2\,r} \\ h_{i-1/2\,r}\, u_{i-1/2+} \end{pmatrix}.$$

The positive parts in the definitions of $h_{i+1/2\,l}$ and $h_{i-1/2\,r}$ (we have $\max(0,\cdot)$) ensure the positivity of the water height. Therefore, the scheme can be written into the form

$$U_i^{n+1} - U_i^n + \frac{\Delta t}{\Delta x}(F_{i+1/2\,l}^n - F_{i-1/2\,r}^n - Fc_i^n) = 0,$$

where

$$F_{i-1/2\,r}^n = \mathcal{F}(U_{i-1/2\,l}^n, U_{i-1/2\,r}^n) + \begin{pmatrix} 0 \\ \frac{g}{2}\left((h_{i-1/2+}^n)^2 - (h_{i-1/2\,r}^n)^2\right) \end{pmatrix},$$

$$F_{i+1/2\,l}^n = \mathcal{F}(U_{i+1/2\,l}^n, U_{i+1/2\,r}^n) + \begin{pmatrix} 0 \\ \frac{g}{2}\left((h_{i+1/2-}^n)^2 - (h_{i+1/2\,l}^n)^2\right) \end{pmatrix},$$

and

$$Fc_i^n = \begin{pmatrix} 0 \\ -\frac{g}{2}\left(h_{i-1/2+}^n + h_{i+1/2-}^n\right)\left(Z_{i+1/2-}^n - Z_{i-1/2+}^n\right) \end{pmatrix}.$$

The term Fc_i^n is added to obtain a well-balanced and consistent scheme [23]. Now, to have a second order scheme in time, we use the Heun method,

$$\begin{aligned} \widetilde{U}_i^{n+1} &= U_i^n + \Delta t\, \Phi(U_i^n) \\ \widetilde{U}_i^{n+2} &= \widetilde{U}_i^{n+1} + \Delta t\, \Phi(\widetilde{U}_i^{n+1}) \\ U_i^{n+1} &= \frac{U_i^n + \widetilde{U}_i^{n+2}}{2}, \end{aligned} \tag{3.8}$$

where

$$\Phi(U_i^n) = -\frac{1}{\Delta x}(F_{i+1/2\,l}^n - F_{i-1/2\,r}^n - Fc_i^n).$$

Concerning the Manning friction term, we introduce a semi-implicit treatment of this term [21, 29]. Then, the scheme is modified as follows

- Solve the Shallow Water system

$$U_i^* = U_i^n + \Delta t\, \Phi(U_i^n).$$

- Compute $\widetilde{U}_i^{n+1} = \begin{pmatrix} h_i^{n+1} \\ h_i^{n+1}\, \widetilde{u}_i^{n+1} \end{pmatrix}$ by solving the Manning friction term

$$\begin{pmatrix} h_i^{n+1} \\ h_i^* \dfrac{\widetilde{u}_i^{n+1} - u_i^*}{\Delta t} \end{pmatrix} = S\, f_{\Delta t}(U_i^*) \equiv \begin{pmatrix} h_i^* \\ -gk^2 \dfrac{\widetilde{q}_i^{n+1}|q_i^*|}{h_i^n (h_i^{n+1})^{4/3}} \end{pmatrix}.$$

- Solve the Shallow Water system

$$U_i^{**} = \widetilde{U}_i^{n+1} + \Delta t\, \Phi(\widetilde{U}_i^{n+1}).$$

- Compute $\widetilde{U}_i^{n+2} = \begin{pmatrix} h_i^{n+2} \\ h_i^{n+1}\widetilde{u}_i^{n+2} \end{pmatrix}$ by solving the Manning friction term

$$\begin{pmatrix} h_i^{n+2} \\ h_i^{**} \dfrac{\widetilde{u}_i^{n+2} - u_i^{**}}{\Delta t} \end{pmatrix} = S\, f_{\Delta t}(U_i^{**}).$$

- Compute U_i^{n+2} using the Heun method defined by (3.8).

We now describe the treatment of the boundary conditions at the inflow and the outflow. We denote by b subscript the values on the (fictive) boundary cell and by the index "in" the values in the first cell inside the domain. The normal n is equal to -1 on the left boundary ($x = 0$) and 1 on the right boundary ($x = \ell$).

- A solid wall is modeled by imposing $u_b = -u_{\text{in}}$, $h_b = h_{\text{in}}$, on the condition that the topography be extended horizontally on the fictive cells.

- At the inflow boundary, we impose the discharge q_b satisfying $nq_b < 0$. Because we only consider fluvial flows, the water height h_b is computed using Riemann invariants (e.g., [29, 30]). More precisely, assume that $c = \sqrt{gh}$. It is well known that for the Shallow Water system (3.6), the quantity $u \mp 2c$ is constant along the characteristic $\frac{dx}{dt} = u \mp c$. Thus we have

$$u_b + n \times 2c_b = u_{\text{in}} + n \times 2c_{\text{in}}. \tag{3.9}$$

  Multiplying (3.9) by h_b, we obtain

$$-n \times 2\sqrt{g} h_b^{3/2} + (u_{\text{in}} + n \times 2c_{\text{in}}) h_b - q_b = 0.$$

  Newton method is used to solve the last equation and to get h_b.

- At the outflow boundary, we always impose the water height h_b and we use Riemann invariants to compute the discharge. We obtain

$$u_b = u_{\text{in}} + n \times 2(c_{\text{in}} - c_b)$$

  and we can easily deduce $q_b = h_b\, u_b$.

All the previous steps are usual for the resolution of the Shallow Water system (2.1). Note that, for our new 2D model (2.4), the additional friction term is treated in an explicitly. As the obtained results are satisfactory, we did not try to use a semi-implicit treatment of the additional friction term. Keeping the explicit treatment also allows the numerical model to be extended easily to more complex two-dimensional flows.

4. Numerical results

In Section 2, we introduced several models: the usual Shallow Water system (2.1), the Shallow Water system with an additional friction coefficient that represents the furrows when we consider plane topography (2.4) and a two-layer model (2.5). In this section, we present several results obtained with these three models in order to show the ability of our new model (2.4)

to approximate the exact solution. Namely, we consider two types of test cases: in the first one, we only take into account rainfalls, and in the second one, the water comes from upstream. For these two numerical experiments, the "exact" (or reference) solution is that from the Shallow Water system (2.1) with a precise description of a topography with furrows. The domain Ω we consider here is $\Omega = \ell \times L$, where $\ell = 0.2$ m and $L = 4$ m (Figure 2). We assume that the plane topography has a constant slope of 5%. The amplitude of the furrows is 0.01 m (0.02 m peak-to-peak), and their wavelength is 0.1 m. We choose a friction coefficient $k = 0.04$ m$^{1/3}$ s^{-1}. For the following computations, we use a time step $\Delta t = 0.001$ s (this time step is imposed by the resolution of (2.1), because we need a small space step to get a good representation of the furrows).

We note that all the numerical results are obtained using C++ software for the resolution of the Shallow Water system, and a new library for the new friction coefficient.

4.1. Reference solutions and description of the test cases

This paragraph describes how the solutions of the Shallow Water model (2.1) are computed when the geometry of the furrows is known explicitly. These solutions will be considered here as reference solutions. According to the parameters given above, the topography is modeled by the equation:

$$Z(x, y) = -0.05\, y + 0.01 \cos(20\pi\, y). \tag{4.10}$$

The space steps (with respect to x and y) are equal to 0.01 m, which means that each furrow is described by 200 cells. We assume that the domain is initially empty, i.e., $\boldsymbol{u}(0, \boldsymbol{x}) = \mathbf{0}$ and $h(0, \boldsymbol{x}) = 0$.
Let h, u, and q denote these reference solutions at the small scale.

4.1.1. Rainfall test case

In this case, we impose rainfall on the whole domain with a constant permanent rain intensity $R = 8 \times 10^{-4}$ m s^{-1}. The rain discharge is then $Q_R = 3.2 \times 10^{-3}$ m^2 s^{-1}. The final time is $T = 22.5$ s. Note that because we are interested in the effects of the furrows, we focus on the transitional stage of the flow. Therefore, the final time T is chosen such that the outflow discharge is approximately equal to half of the rain discharge. We assume here that the upstream boundary is a solid wall. We show the side-view of the water height at the final time in Figure 5 .

4.1.2. Inflow test case

We also consider a permanent inflow from upstream. We set $Q_I = 3.132 \times 10^{-2}$ m^2 s^{-1} as discharge on the inflow boundary. The final time is $T = 27.75$ s. As for the rainfall test case, the final time was chosen such that the outflow discharge at T was approximately equal to half of the inflow discharge. We show the side-view of the water height at the final time in Figure 6.

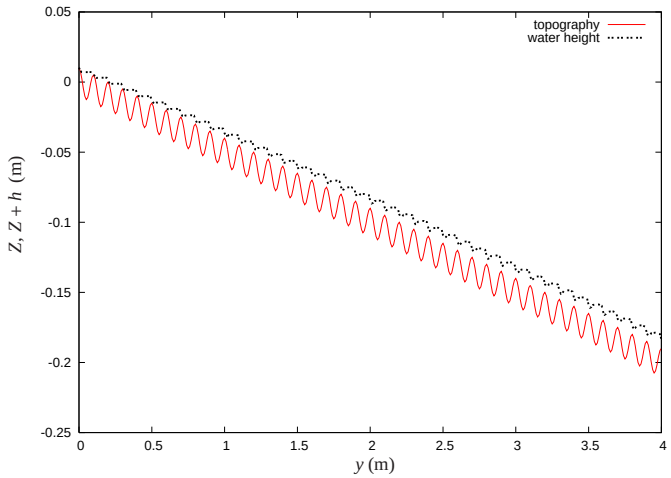

Figure 5: Side-view of the water height at the final time for the rainfall test case.

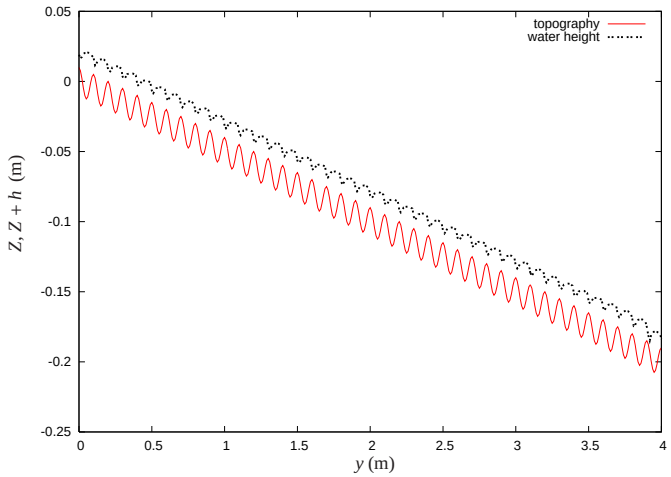

Figure 6: Side-view of the water height at the final time for the inflow test case.

4.2. Numerical comparisons of the models

We perform numerical tests on the new model (2.4). The furrows are removed from the topography defined by (4.10). Thus, the topography is now reduced to an inclined plane with the same general slope:

$$Z(x, y) = -0.05\, y. \tag{4.11}$$

The space step with respect to y is set equal to the wavelength of the furrows, i.e., 0.1 m. The initial conditions remain unchanged: $\boldsymbol{u}(0, \boldsymbol{x}) = \mathbf{0}$ and $h(0, \boldsymbol{x}) = 0$. The capital letters (H, U and Q) denote the solutions of (2.4) at the large scale.

To improve the comparison in the rainfall test, we also compute the solution (h,u,q) of the two-layer system (2.5). The discretization parameters and the topography we use are the same as for the system (2.4).

To compare the three models (2.1), (2.4) and (2.5), we consider the water height (h, H and h, respectively) and the discharge (q, Q and q, respectively) at the outflow. For this purpose, we first introduce $\overline{h^n}^i$ as the average of the reference water

height h contained in the furrow i at the time t^n. We also consider H_i^n, the water height in the furrow i at time t^n, which is computed with the model (2.4) for a given K_0 and a given C, and $H_{0_i}^n$ in the case $K_0 = 0$ (i.e., the Shallow Water system on the coarser grid with plane topography and without the new friction term). Next, we denote by e^H the relative water height error defined by

$$e^H = \left(\frac{\sum_{n=1}^{N} \sum_i \left| \overline{h^n}^i - H_i^n \right|^2}{\sum_{n=1}^{N} \sum_i \left| \overline{h^n}^i - H_{0_i}^n \right|^2} \right)^{1/2}, \tag{4.12}$$

where $t^N = T$ is the final time of the simulations. This error represents the effect of the new friction term $K(h)$ in system (2.4) on the water height.

Finally we also study the discharge at the outflow: if q^n is the value of q (from the resolution of (2.1) with the explicit topography) at time t^n, for $y = L$, Q^n and Q_0^n are the solutions of (2.4) for given K_0 and C, and for $K_0 = 0$, respectively, then the discharge error e^Q is defined by:

$$e^Q = \frac{\sum_{n=1}^{N} |q^n - Q^n|}{\sum_{n=1}^{N} \left| q^n - Q_0^n \right|}. \tag{4.13}$$

The value of e^Q shows the influence of the term $K(h)$ on the discharge at the outflow.

4.2.1. Rainfall test case

For the rainfall test case (Section 4.1.1), we present the water height error e^H between models (2.1) and (2.4), as a function of K_0 for $C = 10$ in Figure 7. We started with a step of 0.01 until $K_0 = 0.1$, and then the step is set to 0.1 as the function increases. We remark that the minimum of the error $e^H \simeq 0.2518$ is obtained for $K_0 = 0.02$.

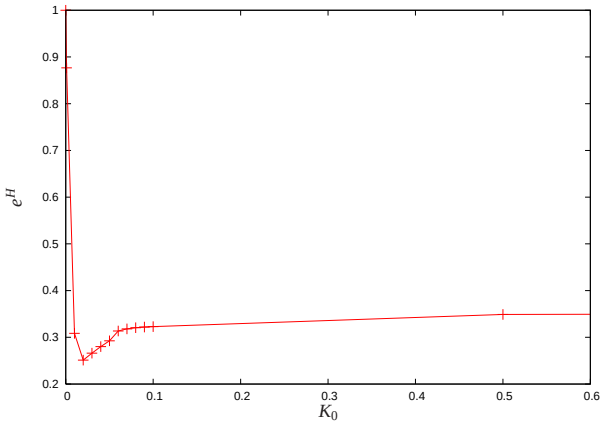

Figure 7: Water height error e^H for the model (2.4) for the rainfall test case.

Then, by optimizing this error with respect to the two parameters K_0 and C, we finally find the minimum $e^H \simeq 0.1417$, which corresponds to $K_0 = 0.02$ and $C = 0.4$. The corresponding discharge error is $e^Q \simeq 5.8 \times 10^{-2}$. We notice that the new model (2.4) allows the L^2 error on the water height to diminish by a factor of 7 with respect to the case $K_0 = 0$, which indicates that the furrow effects are taken into account satisfactorily.

We now report the results obtained with the two-layer model (2.5), for the rainfall test. For different Manning coefficients k, Figure 8 shows the water height error e^{h} (obtained by replacing the solution H of system (2.4) by the solution h of (2.5) in (4.12)). The objective of this test is to understand how the changes in the Manning coefficient combined with a delay at the beginning of the experiment can represent the effects of the furrows. We note that the minimum is $e^{\mathrm{h}} \simeq 0.0422$ for $k = 0.03$. The corresponding discharge error is $e^Q \simeq 8.6 \times 10^{-3}$. We also note that the two-layer model allows the L^2 error on the water height to diminish by a factor of 23 with respect to model (2.4) for the case $K_0 = 0$.

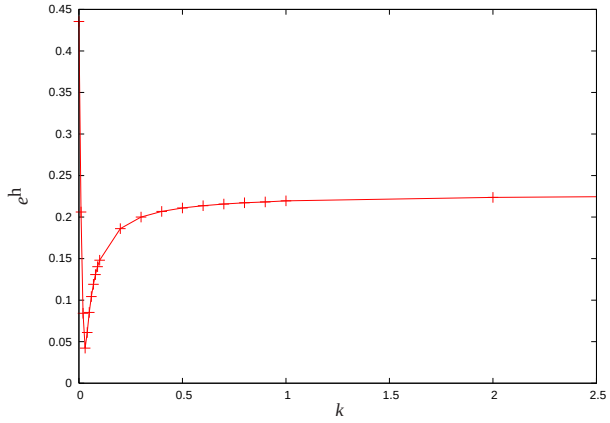

Figure 8: Water height error e^{h} for the two-layer model (2.5).

The first conclusion of this rainfall test is that the two proposed models (2.4) and (2.5) are good representations of the effects of the furrows because their error is smaller than the one of the plane topography model. More precisely, the two-layer model seems better on this test, but as we mentioned before, its extension to the general two dimensional case is not obvious.

To complete this test case, we directly compare the results of the three models. Figure 9 gives the ratio between the computed outflow discharge and the rain discharge for all the models as a function of time. We plot four results in the transitory regime: the discharge computed with (2.4) with $K_0 = 0.02$ and $C = 0.4$, the discharge with $K_0 = 0$, the solution of (2.5) with $k = 0.03$ and the reference solution q (Section 4.1).

Although the domain in the new model (2.4) is an inclined plane, we observe that the additional friction term is able to retain the water for a moment during the rainfall. It is a good approximation to simulate the existence of the furrows.

4.2.2. Inflow test case

Now we consider the inflow test case (Section 4.1.2), and we conduct the same study as for the rainfall test to validate our new model of friction coefficient model. Figure 10 shows the water height error e^H between models (2.1) and (2.4) as a

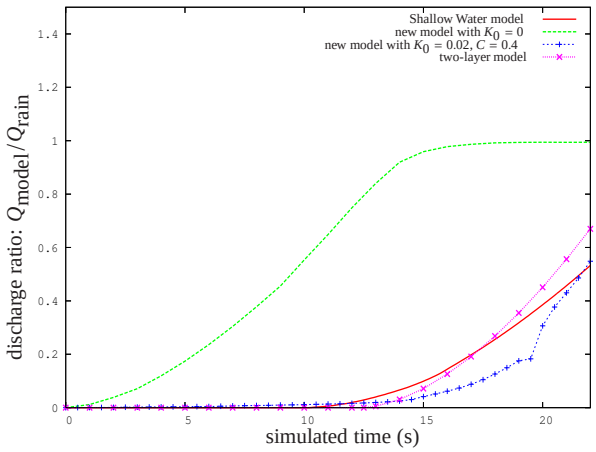

Figure 9: Ratio between the outflow discharge and the rain discharge for all the models as a function of time.

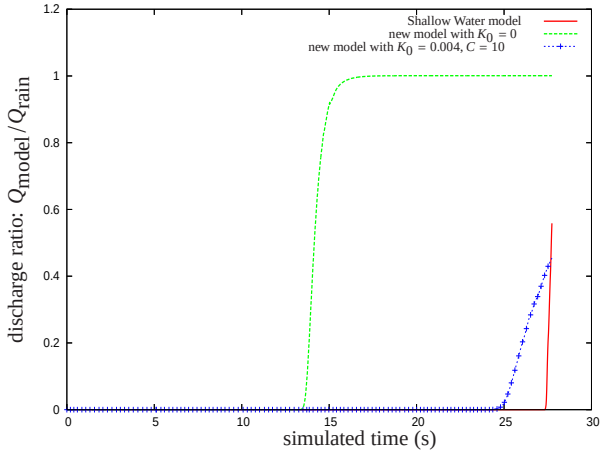

Figure 11: Ratio between the outflow discharge and the imposed inflow discharge for all the models as a function of time.

function of K_0 for $C = 10$. The step on K_0 is set equal to 0.001 when the error is decreasing and 0.01 for larger errors. We note that the minimum error is $e^H \simeq 0.3211$ for $K_0 = 0.004$. The corresponding discharge error is $e^Q \simeq 4.4668 \times 10^{-2}$. We note that our new model (2.4) reduces the L^2 error on the water height by a factor of 1.62 with respect to the case $K_0 = 0$.

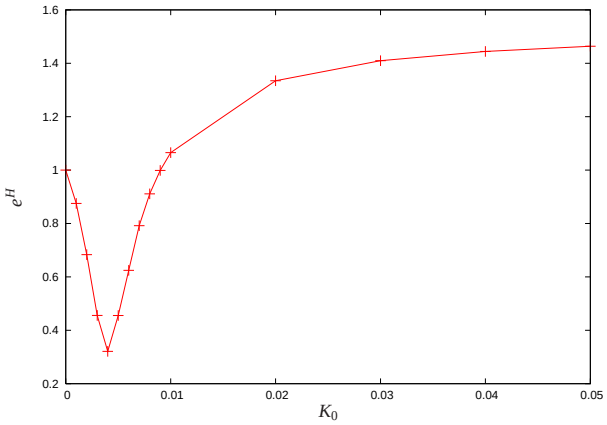

Figure 10: Water height error e^H for the model (2.4) for the inflow test case.

We also present in Figure 11 the ratio between the outflow discharge Q^n, Q_0^n and the imposed inflow discharge at the transitory regime, for the model (2.4) with $K_0 = 0.004$, $C = 10$ and $K_0 = 0$, respectively, and for the reference solution q computed in Section 4.1.
Here too, we observe that the new model simulates the effect of the furrows well.

Remark 4.1. *We do not address the optimization of the value of C because the optimized coefficient for K_0 is ten times smaller than that for the rainfall test, and so the results do not visibly vary when we change C.*

4.2.3. Performance of the new model with calibrated coefficients

In the previous section, the numerical experiments show that our new model (2.4) with the additional friction coefficient that represents the furrows provides good results on the water height and the outflow discharge compared to the reference solution computed on the explicit topography. However, this model requires calibrating the two coefficients K_0 and C. In this section, we study the robustness of this calibration when we change numerical (the space step) or physical (the slope or the roughness of the domain) parameters.

In this part, we only consider the rainfall test case and, as explained before (Section 4.2.1), we choose $K_0 = 0.02$ and $C = 0.4$. Consequently, in the following, we study the performance of the model (2.4) with these values.

For a future extension to fully two-dimensional problems, the new model has to predict the flow directions on each grid cell over the area of agricultural fields. As a consequence, the dimension of a grid cell can vary from 1 to 100 m^2. Thus, a grid cell typically contains several furrows. To test for this scale effect, we present the relative errors e^H and e^Q to the reference solution as functions of the space step in Table 1. This space step varies from 0.1 m to 0.4 m which means that a cell comprises 1–4 furrows. We note that the variation of the error e^H is small; when the space step is multiplied by 4, the relative error is multiplied by less than 1.5.

Space step (m)	e^H	e^Q	CPU time
0.1	0.1417	5.8×10^{-2}	0.11
0.2	0.1675	7.2865×10^{-2}	0.0574
0.4	0.2024	8.963×10^{-2}	0.0255

Table 1: Relative errors of the water height and the flowrate, and CPU times (normalized with respect to the time to compute the reference solution).

We also present the computational times to compute the solutions of the new model in Table 1 (depending on the space step). The values are normalized with respect to the compu-

tational time needed to compute the reference solutions. We observe that the new model reduces the computational time by at least 90% and can easily achieve a 97% decrease under the condition that we tolerate a small error on the solution.

In Table 2, we present the errors e^H and e^Q for different general slopes of the topography (with a realistic range for agricultural fields) for the calibrated values $K_0 = 0.02$ and $C = 0.4$. We note that the new model reduces the L^2 error on the water height by at least a factor of 4 compared to the reference solution, which shows that the effects of the furrows are taken into account satisfactorily.

We complete these results with Table 3, where for each slope, we calibrate the coefficients K_0 and C to get the minimum of the relative error e^H. Comparing the values of the coefficients and of the errors in Tables 2 and 3, we see that the new model with the calibrated values $K_0 = 0.02$, $C = 0.4$ still yields accurate results.

slope	K_0	C	e^H	e^Q
2%	0.02	0.4	0.2434	0.1855
5%	0.02	0.4	0.1417	5.8×10^{-2}
8%	0.02	0.4	0.2194	0.187
11%	0.02	0.4	0.2035	0.171

Table 2: Errors e^H and e^Q for different general slopes of the topography with $K_0 = 0.02$ and $C = 0.4$.

slope	K_0	C	e^H	e^Q
2%	0.02	0.3	0.2167	0.1134
5%	0.02	0.4	0.1417	5.8×10^{-2}
8%	0.04	0.4	0.1205	8.1222×10^{-2}
11%	0.04	0.4	0.1089	6.8554×10^{-2}

Table 3: Minimum errors e^H with the corresponding coefficients K_0, C and the values of e^Q for different general slopes of the domain.

Table 4 shows the errors e^H and e^Q for different Manning coefficients (the slope is kept equal to 5%) for the calibrated values $K_0 = 0.02$ and $C = 0.4$. As for the variation of the slope, in Table 5, we give the coefficients K_0 and C that minimize the relative error e^H for each Manning coefficient, and we complete the table with the corresponding error e^Q. Once more we see that the results given by our model (2.4) are good compared to the reference solution.

The last results we present are dedicated to water heights and discharges errors at steady state for the Shallow Water model (2.1). The final time of the simulations is then $T = t^s = 50$ s. The two models we consider are the new model (2.4) with the calibrated coefficients $K_0 = 0.02$ and $C = 0.4$, and the usual Shallow Water model (2.1) with an explicit description of the topography and of the furrows.

We now denote e_s^H as the water height error at steady state defined by

$$e_s^H = \left(\frac{\sum_i |\overline{h^s}^i - H_i^s|^2}{\sum_i |\overline{h^s}^i - H_{0_i}^s|^2} \right)^{1/2}.$$

Manning coefficient ($m^{1/3}s^{-1}$)	K_0	C	e^H	e^Q
0.001	0.02	0.4	0.0744	4.67×10^{-2}
0.04	0.02	0.4	0.1417	5.8×10^{-2}
0.1	0.02	0.4	0.2746	9.9691×10^{-2}

Table 4: Errors e^H and e^Q for $K_0 = 0.02$ and $C = 0.4$ for different Manning coefficients.

Manning coefficient ($m^{1/3}s^{-1}$)	K_0	C	e^H	e^Q
0.001	0.02	0.4	0.0744	4.67×10^{-2}
0.04	0.02	0.4	0.1417	5.8×10^{-2}
0.1	0.02	0.5	0.265	0.1128

Table 5: Minimum errors e^H with the corresponding coefficients K_0, C and the values of e^Q for different Manning coefficients.

Note that e_s^H has the same definition as e^H (4.12) except that instead of summing the values of the water heights for all the discrete times, we only consider the time corresponding to the steady state t^s.

The value we obtain with the new model is $e_s^H \simeq 0.1765$. Thus, we deduce that at the steady state, the new model (2.4) with the calibrated coefficients takes into account the effects of the furrows and approximates the Shallow Water model (2.1) well.

5. Conclusions

In this paper, we proposed a new Shallow Water model (2.4) to describe the effects of furrows during overland flow without representing them explicitly. The main idea is to include the additional friction term (2.3) that takes into account the effects of these furrows in the classical Shallow Water equations (2.1). The new model is proposed under the assumptions that the flow is fluvial and the direction of the flow is perpendicular to the furrows, parallel to a side of the rectangular domain. We also assumed that there is no infiltration and no soil erosion.

We presented numerical results to show the efficiency and the performance of the new model. We compared it with a two-layer model in which there is a delay due to the filling of the furrows and with which we can assess the behavior of a model with a variable Manning coefficient. Both models give good results for the rainfall test. We also showed that the calibration of the coefficient of the new model does almost not depend on the slope of the domain (Tables 2 and 3) nor on the soil friction coefficient (Tables 4 and 5).

The numerical results presented in this paper are encouraging and indicate that the idea could be extended to more complex two-dimensional flows. This extension is now the main goal of the forthcoming works. Note that, unlike the two-layer model (2.5), the new model (2.4) can easily be generalized to two-dimensional problems. These extensions include the random variations of the height of the furrows. As we mentioned in the description of (2.3), these variations can be taken into account in the constant C of the additional friction term. The extensions also include the case in which the direction of the

furrows is not perpendicular to the slope of the domain; this will lead to study the effects of this direction with respect to the slope.

Acknowledgements

This work was supported by the ANR project METHODE #ANR-07-BLAN-0232 (`http://www.univ-orleans.fr/mapmo/methode/`) and the Région Centre, France. The authors wish to thank the members of the project for their helpful discussions and comments. The authors also want to thank the anonymous referees for their constructive comments and their useful suggestions that improved the paper.

References

[1] K. Beven, On undermining the science?, Hydrol. Process. 20 (2006) 2050–2065.

[2] V. Jetten, A. de Roo, D. Favis-Mortlock, Evaluation of field-scale and catchment-scale soil erosion models, Catena 37 (1999) 521–541.

[3] V. Jetten, G. Govers, R. Hessel, Erosion models: quality of spatial predictions, Hydrol. Process. 17 (2003) 887–900.

[4] V. Souchère, D. King, J. Daroussin, F. Papy, A. Capillon, Effects of tillage on runoff directions: consequences on runoff contributing areas within agricultural catchments, J. Hydrol. 206 (1998) 256–267.

[5] P. Quinn, K. Beven, P. Chevallier, O. Planchon, The prediction of hillslope flow paths for distributed hydrological modelling using digital terrain models, Hydrol. Process. 5 (1991) 59–79.

[6] D. G. Tarboton, A new method for the determination of flow directions and upslope areas in grid digital elevation models, Water Resour. Res. 33 (1997) 309–331.

[7] F. Darboux, P. Davy, C. Gascuel-Odoux, Effect of depression storage capacity on overland-flow generation for rough horizontal surfaces: Water transfer distance and scalling, Earth Surf. Process. Landforms 27 (2) (2002) 177–191.

[8] C. X. Jin, M. J. M. Römkens, F. Griffioen, Estimating Manning's roughness coefficient for shallow overland flow in non-submerged vegetative filter strips, Trans. ASAE 43 (2000) 1459–1466.

[9] J. E. Gilley, D. C. Flanagan, E. R. Kottwitz, M. A. Weltz, Darcy-Weisbach roughness coefficients for overland flow, in: A. J. Parsons, A. D. Abrahams (Eds.), Overland Flow. Hydraulics and Erosion Mechanisms, University College London Press, London, 1992, pp. 25–52.

[10] O. Planchon, M. Esteves, N. Silvera, J. Lapetite, Microrelief induced by tillage: measurement and modelling of Surface Storage Capacity, Catena 46 (2001) 141–157.

[11] I. Takken, G. Govers, V. Jetten, L. Nachtergaele, A. Steegen, J. Poesen, Effect of tillage and runoff and erosion patterns, Soil Tillage Res. 61 (2001) 55–60.

[12] A. J.-C. de Saint-Venant, Théorie du mouvement non-permanent des eaux, avec application aux crues des rivières et à l'introduction des marées dans leur lit, C. R. Math. Acad. Sci. Paris 73 (1871) 147–154, [In French].

[13] J.-F. Gerbeau, B. Perthame, Derivation of viscous Saint-Venant system for laminar shallow water; numerical validation, Discrete Contin. Dyn. Syst. Ser. B 1 (1) (2001) 89–102.

[14] S. Ferrari, F. Saleri, A new two-dimensional shallow water model including pressure effects and slow varying bottom topography, M2AN Math. Model. Numer. Anal. 38 (2) (2004) 211–234.

[15] F. Marche, Derivation of a new two-dimensional viscous shallow water model with varying topography, bottom friction and capillary effects, Eur. J. Mech. B Fluids 26 (1) (2007) 49–63.

[16] M. W. Smith, N. J. Cox, L. J. Bracken, Applying flow resistance equations to overland flows, Progress in Physical Geography 31 (4) (2007) 363–387. doi:10.1177/0309133307081289.

[17] E. Audusse, A multilayer Saint-Venant model: derivation and numerical validation, Discrete Contin. Dyn. Syst. Ser. B 5 (2) (2005) 189–214.

[18] E. Audusse, M.-O. Bristeau, Finite-volume solvers for a multilayer Saint-Venant system, Int. J. Appl. Math. Comput. Sci. 17 (3) (2007) 311–319.

[19] M. Castro, J. Macías, C. Parés, A *Q*-scheme for a class of systems of coupled conservation laws with source term. Application to a two-layer 1-D shallow water system, M2AN Math. Model. Numer. Anal. 35 (1) (2001) 107–127.

[20] M. Esteves, X. Faucher, S. Galle, M. Vauclin, Overland flow and infiltration modelling for small plots during unsteady rain: numerical results versus observed values, J. Hydr. 228 (2000) 265–282.

[21] R. F. Fiedler, J. A. Ramirez, A numerical method for simulating discontinuous shallow flow over an infiltrating surface, Int. J. Num. Meth. Fluids 32 (2000) 219–240.

[22] J. Greenberg, A.-Y. Le Roux, A well-balanced scheme for the numerical processing of source terms in hyperbolic equation, SIAM J. Num. Ana. 33 (1996) 1–16.

[23] E. Audusse, F. Bouchut, M.-O. Bristeau, R. Klein, B. Perthame, A fast and stable well-balanced scheme with hydrostatic reconstruction for shallow water flows, SIAM J. Sci. Comput. 25 (6) (2004) 2050–2065.

[24] F. Bouchut, Nonlinear stability of finite volume methods for hyperbolic conservation laws and well-balanced schemes for sources, Frontiers in Mathematics, Birkhäuser Verlag, Basel, 2004.

[25] O. Delestre, S. Cordier, F. Darboux, F. James, Simulation of rain-water overland-flow, in: E. Tadmor, J.-G. Liu, A. Tzavaras (Eds.), Hyp2008 — Proceedings of the 12th International Conference on Hyperbolic Problems: Theory, Numerics, Applications, Vol. 67 of Proceedings of Symposia in Applied Mathematics, University of Maryland, American Mathematical Society, Providence, Rhode Island, USA, 2009, pp. 537–546. URL `http://www.ams.org/bookstore-getitem?item=PSAPM-67`

[26] O. Delestre, F. James, Simulation of rainfall events and overland flow, in: Proceedings of X International Conference Zaragoza-Pau on Applied Mathematics and Statistics, Jaca, Spain, september 2008, Monografías Matemáticas García de Galdeano, available at http://hal.archives-ouvertes.fr/hal-00426694/fr/, 2009, pp. 125–135.

[27] O. Delestre, Rain water overland flow on agricultural fields simulation, Ph.D. thesis, Université d'Orléans, [In French], available at http://tel.archives-ouvertes.fr/tel-00531377_v1/ (2010).

[28] F. Bouchut, Efficient numerical finite volume schemes for shallow water models, in: Ziet lin, V., editor, Nonlinear Dynamics of Rotating Shallow water : Methods and Advances, volume 2 of Edited Series on Advances in Nonlinear Science and Complexity, Elsevier Science, 2007, pp. 189 – 256.

[29] M.-O. Bristeau, B. Coussin, Boundary conditions for the shallow water equations solved by kinetics schemes, Inria report RR-4282, available at http://hal.inria.fr/inria-00072305/en/.

[30] J. Lhomme, One-dimensional, two-dimensional and macroscopic approaches to urban flood modelling, Ph.D. thesis, Université Montpellier II, [In French], available at http://tel.archives-ouvertes.fr/tel-00389236/fr/ (2006).